

## Supporting Information

# A fluoride-incorporated composite electrolyte enabling high-voltage all-solid-state sulfide-based lithium metal batteries

### Experimental Section

#### 1 Sample synthesis

The raw materials used to synthesize the  $\text{Li}_{5.5}\text{PS}_{4.5}\text{Cl}_{1.5}$  solid-state electrolyte were  $\text{Li}_2\text{S}$  (Aladdin,  $\geq 99.8\%$ ),  $\text{P}_2\text{S}_5$  (Macklin,  $\geq 99\%$ ), and  $\text{LiCl}$  (Macklin,  $\geq 99.9\%$ ).  $\text{Li}_2\text{S}$ ,  $\text{P}_2\text{S}_5$ , and  $\text{LiCl}$  were weighed based on the reaction stoichiometry equation and ball-milled for 16 hours at 500 rpm using WC balls in a planetary mill. The produced powders were then sintered in a muffle furnace with a heating rate of  $2\text{ }^\circ\text{C min}^{-1}$  for 6 hours at  $500\text{ }^\circ\text{C}$ .  $\text{AlF}_3$  (Aladdin,  $\geq 99.9\%$ ) and  $\text{LiF}$  (Aladdin,  $\geq 99.9\%$ ) were weighed and then milled at 500 rpm in a WC mill tank for 24 hours to prepare  $\text{Li}_3\text{AlF}_6$ . Subsequently, the targeted composite electrolyte  $x\text{Li}_3\text{AlF}_6\text{-(1-x) Li}_{5.5}\text{PS}_{4.5}\text{Cl}_{1.5}$  was synthesized by milling  $\text{Li}_3\text{AlF}_6$  electrolyte with the  $\text{Li}_{5.5}\text{PS}_{4.5}\text{Cl}_{1.5}$  electrolyte at a particular mass ratio in a planetary mill for 3 hours at a speed of 500 rpm. The entire synthesis process was conducted under an argon atmosphere.

#### 2 Electrochemical measurements

The entire battery fabrication process was carried out inside a glovebox filled with argon gas. The synthesized electrolyte powder was pressed into a thin pellet (weighing 100 mg) under a pressure of 450 MPa using a mold. The ionic conductivity of the pellet was tested over a frequency range of 2 MHz to 0.1 Hz at a voltage of 50 mV using the electrochemical workstation (Squidstat Plus, Admiral). The same pressing method and testing equipment were employed for the direct current (DC) polarization test, in which a voltage of 0.5 V was applied for a duration of 6000 s to measure the electronic conductivity of the sample. The target electrolyte was mixed with VGCF (vapor-grown carbon fiber) at a mass ratio of 9:1 and milled in a  $\text{ZrO}_2$  milling jar at 200 rpm for 1 h. The obtained powder was used as the cathode. A composite pellet was prepared by layer-pressing 30 mg of the target electrolyte with 70 mg of  $\text{Li}_{5.5}\text{PS}_{4.5}\text{Cl}_{1.5}$  electrolyte at 450 MPa. A Li-In (lithium-indium) alloy was used as the anode. The assembled battery for LSV (linear sweep voltammetry) testing was as follows: composite cathode (10 mg)/target electrolyte (30 mg)/  $\text{Li}_{5.5}\text{PS}_{4.5}\text{Cl}_{1.5}$  electrolyte (70 mg)/Li-In anode. The LSV test was performed using an electrochemical workstation (Squidstat Plus, Admiral) to record the current variation as the potential was swept from the initial potential (0 V) to the final potential (6 V) at a scan rate of  $0.1\text{ mV s}^{-1}$ . For the fabrication of the composite cathode for battery performance testing, the target electrolyte was mixed with  $\text{LiCoO}_2$  at a mass ratio of 3:7 and milled in a  $\text{ZrO}_2$  milling jar. Unlike the assembly battery for LSV (linear sweep voltammetry) testing, the loading of the composite cathode in all-solid-state batteries was fixed at 4 mg. The charge-discharge performance, cycling stability, and other tests of the all-solid-state batteries within specific voltage ranges or at different rates were conducted using a NEWARE CT-400 battery tester. To enhance the accuracy of the in-situ impedance tests, the loading of the composite cathode in the all-solid-state batteries was increased to 8 mg, and the cycling protocol was set to 20 cycles at a rate of 0.2C.

#### 3 Materials characterization

The diffraction spectra of the sample was analyzed using an X-ray diffractometer (Rigaku, SmartLab-SE) equipped with a Cu K $\alpha$  radiation source. The measurement was performed over a  $2\theta$  range of  $10^\circ\text{--}80^\circ$  at a scanning speed of  $5.0^\circ\text{ min}^{-1}$ . Raman spectra of the samples were collected by LabEAM HR800 and measured in a vacuum capillary using a 532 nm Laser light source. X-ray photoelectron spectroscopy (XPS) was conducted using K-Alpha+ spectrometers (Thermo Fisher Scientific). Scanning electron microscopy coupled with energy-dispersive spectroscopy (SEM-EDS) was employed to capture images of the surface

morphology and elemental distribution of the samples by TESCAN FSEM-5. High-resolution images and elemental mapping were obtained using a transmission electron microscope (TEM, Talos F200X from Thermo Fisher Scientific).

#### 4 Data analysis

In electrochemical research, the development of interrelated relationships between the frequency and time domains is made possible by the distribution of relaxation times (DRT), an analytical technique that is independent of any particular model. This method enhances the way that the electrochemical impedance spectroscopy (EIS) spectra characterize the relationship between impedance and time constant. Eqs. 1 and 2 reveal the derived relationship between cell impedance and the corresponding DRT<sup>1,2</sup>.

$$\int_0^{\infty} g(\tau) d\tau = 1 \quad (1)$$

$$Z(\omega) = R_0 + Z_{pol}(\omega) = R_0 + R_{pol} \int_0^{\infty} \frac{g(\tau)}{1 + j\omega\tau} d\tau \quad (2)$$

where  $Z(\omega)$  represents the impedance data,  $R_0$  denotes the ohmic impedance,  $Z_{pol}(\omega)$  refers to the polarization impedance,  $R_{pol}$  is the polarization resistance, and  $g(\tau)$  is the associated distribution of relaxation times.

The attained electrochemical impedance spectroscopy can be transformed into a relaxation function  $\gamma(\tau)$ , in which the occurrence of pertinent electrochemical processes is demonstrated by distinct peaks that correspond to particular relaxation times. The impedance values at those particular relaxation times are directly correlated with the area under each peak.

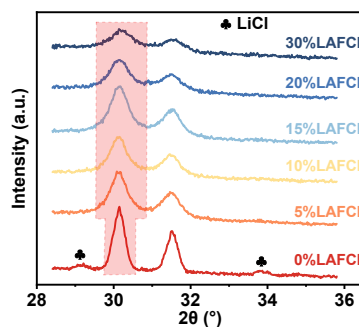


Fig. S1 Details of XRD patterns of LAFCl composite electrolytes prepared by milling with different ratios.

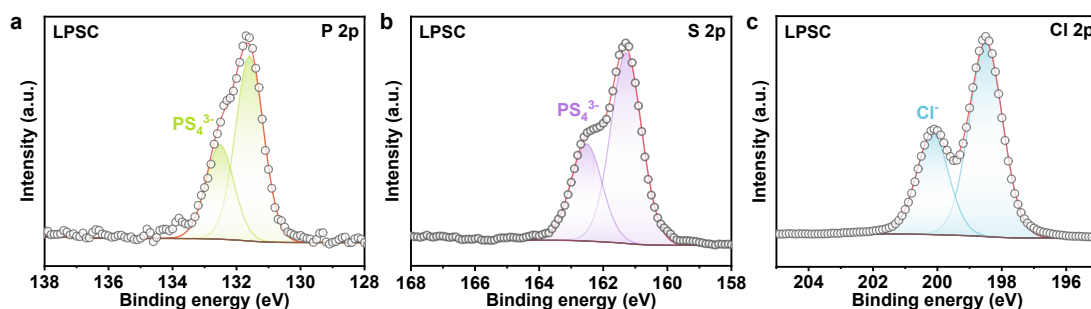


Fig. S2 XPS spectra of  $\text{Li}_{5.5}\text{PS}_{4.5}\text{Cl}_{1.5}$  electrolyte with (a) P 2p, (b) S 2p, and (c) Cl 2p.

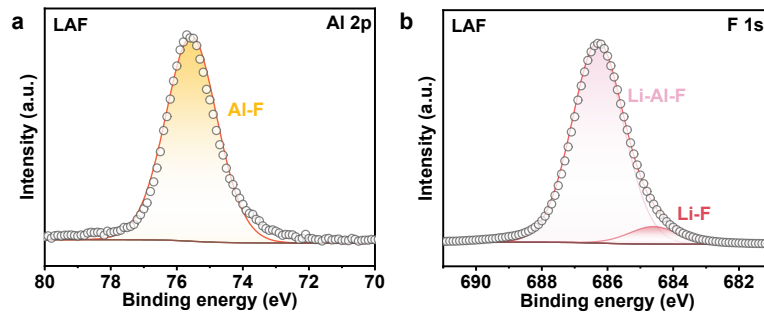


Fig. S3 XPS spectra of  $\text{Li}_3\text{AlF}_6$  electrolyte with (a) Al 2p and (b) F 1s.

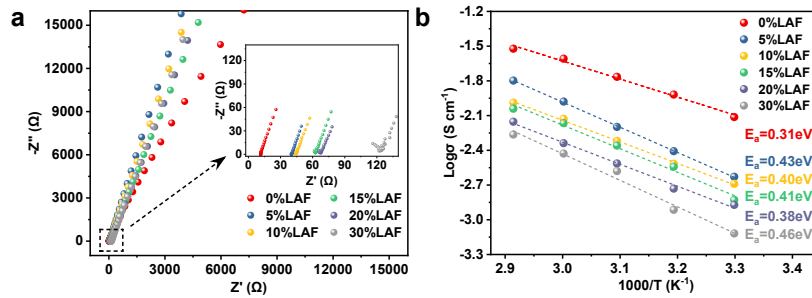


Fig. S4 (a) EIS spectra of composite electrolytes with different LAF doping amounts. (b) corresponding Arrhenius plots at 30°C-70°C temperature.

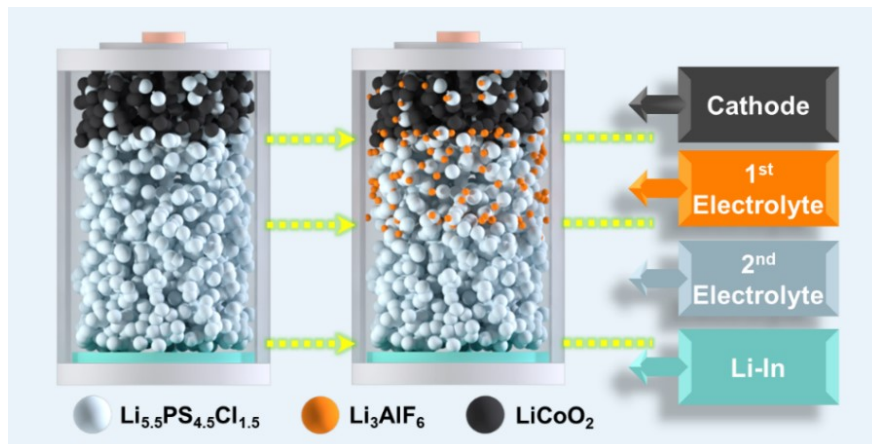


Fig. S5 Schematic diagram of the structural optimization process for high-voltage-adaptive all-solid-state lithium-indium batteries.

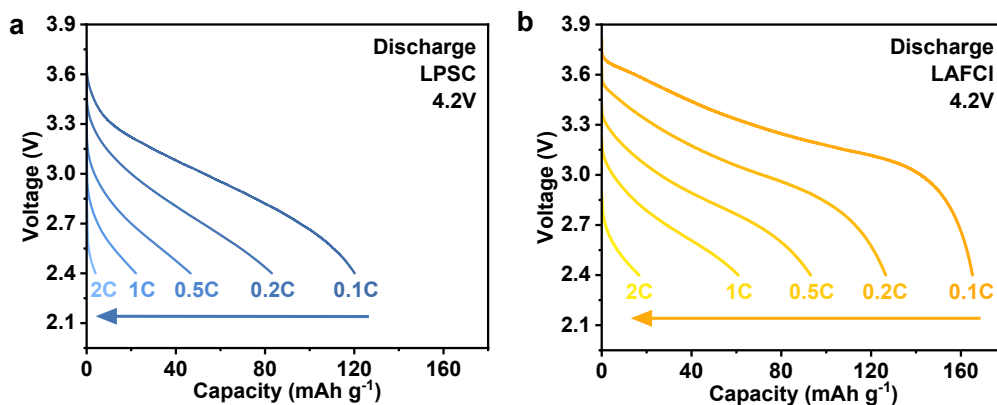


Fig. S6 Discharge curves of (a) LCO/LPSC/Li-In and (b) LCO/LAFCl/LPSC/Li-In batteries at different discharge rates.

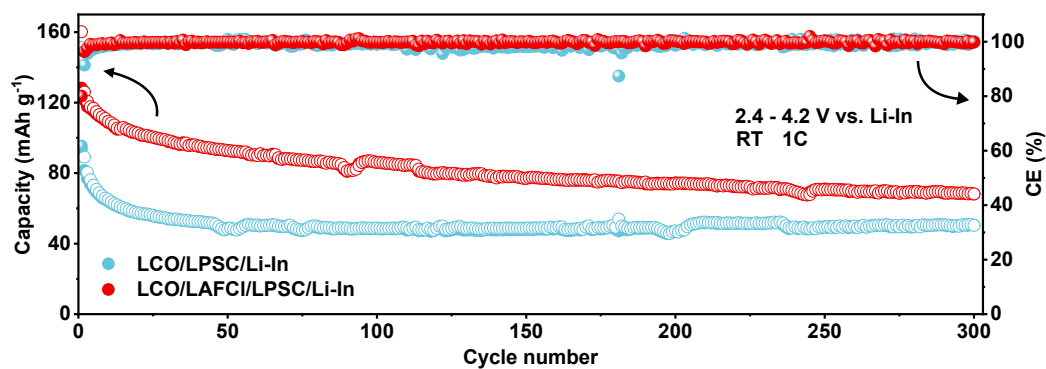


Fig. S7 Cycling stability and Coulombic efficiency of the LCO/LPSC/Li-In and LCO/LAFCl/LPSC/Li-In batteries at 1C for 300 cycles.

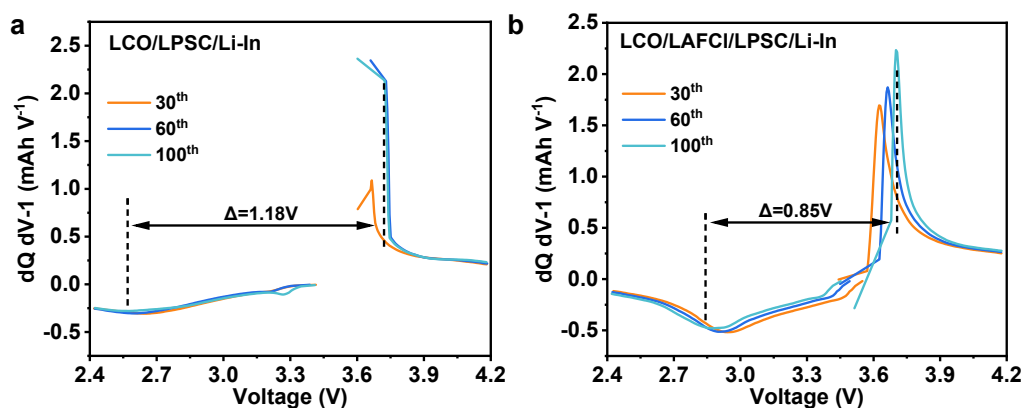


Fig. S8 Polarization voltage difference of (a) LCO/LPSC/Li-In battery and (b) LCO/LAFCl/LPSC/Li-In battery after cycling.

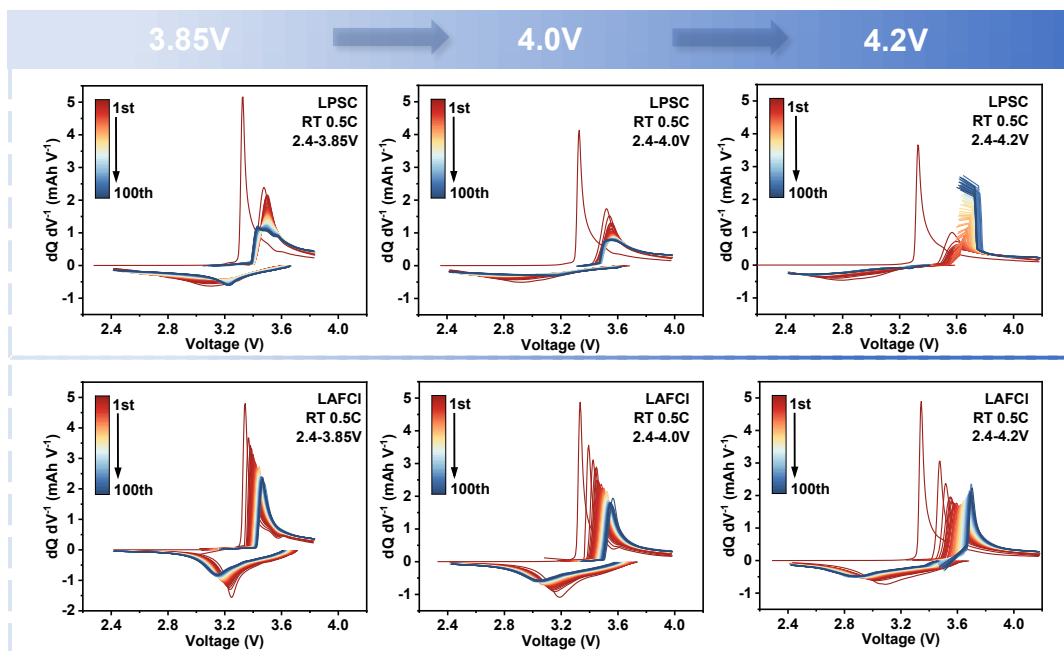


Fig. S9 Differential capacity evolution behavior of LCO/LPSC/Li-In battery and LCO/LAFCl/LPSC/Li-In battery at different upper cutoff voltages (vs. Li-In).

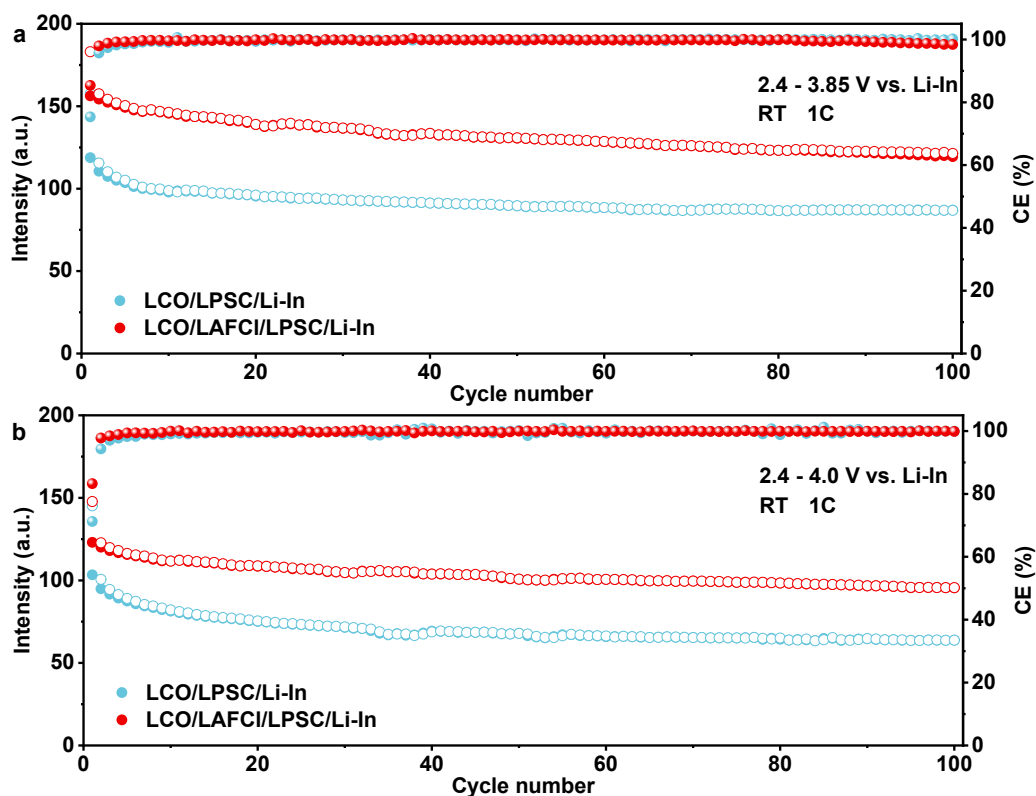


Fig. S10 Cycling stability and Coulombic efficiency of the LCO/LPSC/Li-In and LCO/LAFCl/LPSC/Li-In batteries at 1C.

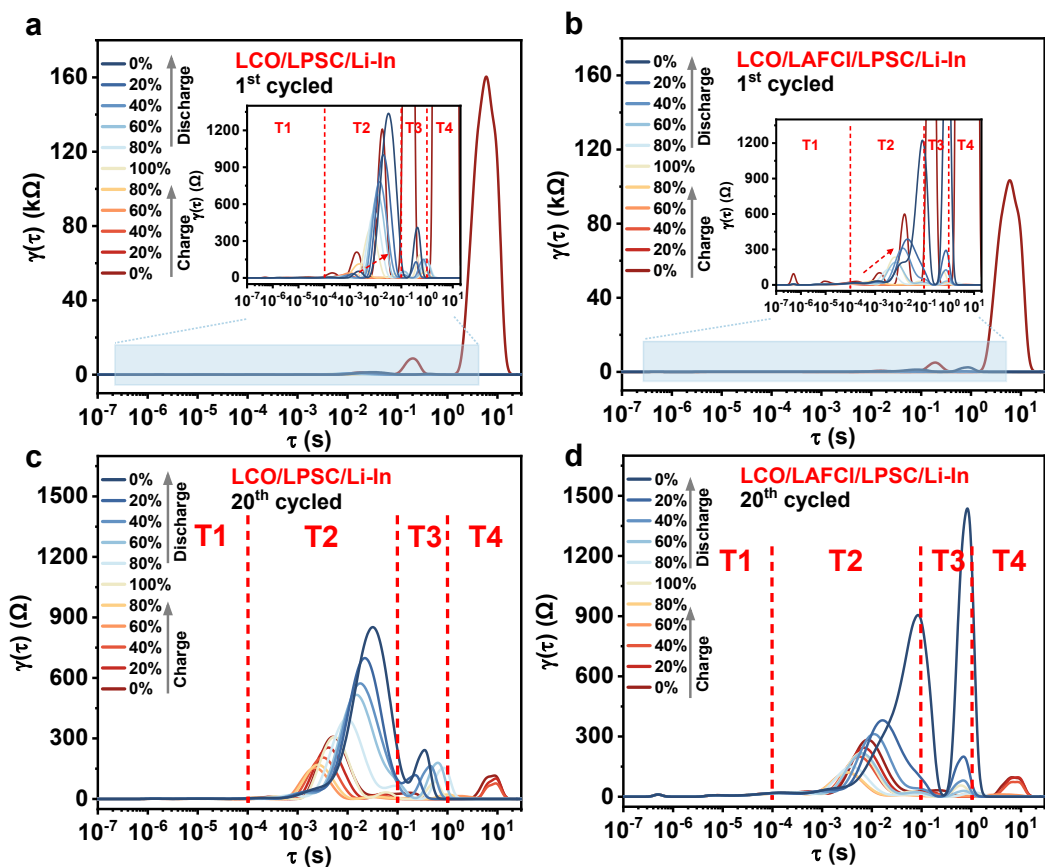


Fig. S11 DRT curves of LCO/LPSC/Li-In battery at (a) 1<sup>st</sup> cycle and (c) 20<sup>th</sup> cycle. And corresponding DRT curves of (b, d) LCO/LAFCl/LPSC/Li-In batteries.

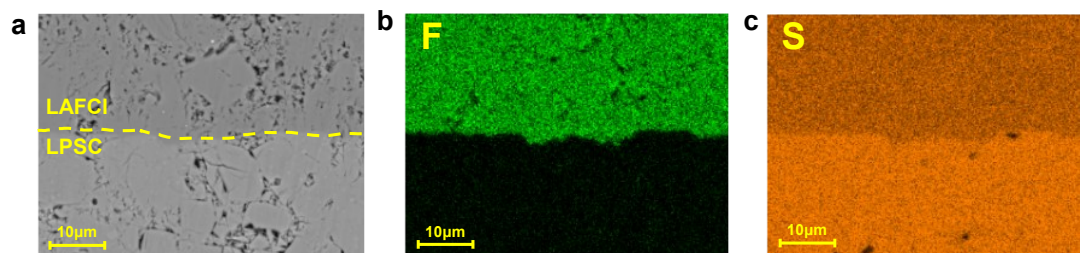


Fig. S12 (a) SEM image and (b, c) EDS mapping of the bilayer electrolyte interface in the batteries cross-section after cycling.

## References

1. D. Y. Semerukhin, A. V. Kubarkov, V. G. Sergeyev, O. A. Semenikhin and E. V. Antipov, *Electrochim. Acta*, 2024, **486**.
2. Y. Lu, C.-Z. Zhao, J.-Q. Huang and Q. Zhang, *Joule*, 2022, **6**, 1172-1198.